3rd European supercritical CO2 Conference
September 19-20, 2019, Paris, France

2019-sCO2.eu-142

EFFECT OF IMPURITIES ON SUPERCRITICAL CO_2 COMPATIBILITY

Bruce A. Pint*
Oak Ridge National Laboratory
Oak Ridge, TN 37831-6156 USA
Email: pintba@ornl.gov

Kinga A. Unocic
Oak Ridge National Laboratory
Oak Ridge, TN 37831-6156 USA

James R. Keiser
Oak Ridge National Laboratory
Oak Ridge, TN 37831-6156 USA

ABSTRACT

Impurities may affect structural alloy compatibility in both indirect- and direct-fired supercritical CO_2 (sCO_2) cycles for high efficiency power generation with peak temperatures above 700°C. Using a new multi-pump gas control system, experiments with controlled impurity additions were compared to baseline results in research- or industrial-grade CO_2 at 750°C/300 bar. Low level impurities, 50 ppm O_2 and 50 ppm H_2O, were not found to affect mass change or reaction products after 2,500 h exposures. However, in RG sCO_2+1%O_2+ 0.25%H_2O, higher reaction rates were observed for both Ni- and Fe-based alloys, but especially Fe-based alloys were strongly affected by these high impurity levels. Analytical TEM was used to characterize the reaction products on alloy 625.

INTRODUCTION

Supercritical CO_2 (sCO_2) could be used as a working fluid for a variety of power generation applications because of its unique properties and relatively low critical point (31°C/74 bar) compared to water [1-4]. Subcritical CO_2 (43 bar) was used in the UK advanced gas cooled reactors (AGR), however, additives such as CH_4, were used to keep the O_2 partial pressure low to minimize graphite oxidation in the reactor core, which increased the C activity [5,6]. Thus, the AGR conditions are very different than those expected for sCO_2. While a range of peak temperatures is being considered for the various sCO_2 applications, CSP and fossil energy desire efficiencies over 50% and require >700°C for indirect-fired or closed cycles [7]. Direct-fired cycles also are targeting similar temperatures [4]. Most studies have shown relatively good compatibility for Ni-based structural alloys needed for >700°C applications in autoclaves using relatively high-purity CO_2 [8-17]. However, the role of impurities in sCO_2 compatibility has not been resolved, either for the low impurity levels in indirect-fired cycles or the higher residual O_2 and H_2O from combustion in the direct-fired cycles [4]. (In addition, S and Cl could be present if coal-derived synthesis gas were combusted.) For example, O_2 additions have shown slightly negative effects [12,14] or little effect [15]. A recent publication provided an initial indication that pressure affects the role of impurities at 750°C/300 bar [17]. This paper provides additional characterization from that study and compares the results to a second experiment where low levels of O_2 and H_2O were intentionally added to simulate the highest impurity levels that might be found in IG CO_2. The structural alloys investigated included two advanced austenitic steels, an alumina-forming Ni-based superalloy (typically used for turbomachinery) and both SS and PS [18,19] Ni-based alloys identified by AUSC [20] for applications above 700°C. These impurity levels at 30 MPa increased the specimen mass change, particularly for the Fe-based alloys.

PROCEDURE

The alloys compared in this study and their measured compositions are shown in Table 1. Coupons (~12 x 20 x 1.5mm) were polished to a 600 grit finish and cleaned in acetone and methanol prior to exposure. All exposures used 500-h cycles at 750°C. Baseline exposures in laboratory air (~50% relative humidity) were conducted in a box furnace with heating for ~4 h and furnace cooling in air. For the 300 bar exposures, the experiments were conducted in an alloy 282 autoclave (~266 mm x 83 mm inner diameter) described previously [10,13]. Specimens were held on an alloy 282 sample rack and slowly heated to temperature over several hours (~2°C/min) in sCO_2, held at temperature ±2°C and then cooled in sCO_2 to room temperature by lowering the furnace and using a cooling fan on the autoclave. In all cases, the fluid flow rate was ~2 ml/min. Experiments were conducted in RG (4.1±0.7 ppm H_2O, <5 ppm O_2) and IG (18.8±16.9 ppm H_2O, <50 ppm O_2) CO_2 [17]. Two autoclaves were modified to use three pumps to deliver sCO_2,

* corresponding author(s)

DOI:10.17185/duepublico/48899

Table 1: Chemical composition of the alloys measured by ICP and combustion analyses in mass% [17].

Alloy	Fe	Ni	Cr	Al	Other
25 SS	42.6	25.4	22.3	0.03	3.4W,3Cu,1.5Co,0.5Mn,0.5Nb
310HN	51.3	20.3	25.5	<	0.3Co,0.4Nb,1.2Mn,0.3Si,0.3N
625	4.0	61.0	21.7	0.1	8.8Mo,3.5Nb,0.2Ti,0.2Mn
230	1.5	60.5	22.6	0.3	12.3W,1.4Mo,0.5Mn,0.4Si
617B	1.2	54.6	22.3	1.0	11.9Co,8.2Mo,0.4Ti,0.04Mn
282 (#1)	0.2	57.1	19.6	1.6	10.6Co,8.6Mo,0.04Si,2.2Ti
282 (#2)	0.2	57.7	19.4	1.6	10.5Co,8.3Mo,0.05Si,2.1Ti
740	0.1	49.7	24.5	1.4	20.6Co,1.5Nb,1.4Ti,0.3Mn
247	0.07	59.5	8.5	**5.7**	9.8Co,10W,0.7Mo,3.1Ta,1.4Hf

< indicates below the detectability limit of 0.01%

CO_2-O_2 and H_2O [17]. Based on the gas flow rate, the O_2 level was calculated as 1.0±0.2% and the H_2O content as 0.25±0.05% for the high impurity experiment. For the low impurity experiment, 50ppm O_2 and 50 ppm H_2O were targeted.

For all experiments, specimen mass change was measured using a Mettler Toledo model XP205 balance with an accuracy of ~±0.04 mg or 0.01 mg/cm^2. After exposure, samples were copper plated before being sectioned and mounted for light microscopy. Both oxide thickness and internal oxidation were measured using image analysis software with ~20-30 measurements taken for each specimen. Prior publications reported characterization using SEM and GDOES. Recent results using STEM/EDS are reported. The TEM specimens were prepared via the *in situ* FIB lift-out method on a Hitachi model NB5000 FIB-SEM. A W layer was deposited to protect the gas interface of the scale. The STEM imaging was carried out using a FEI model Talos F200X STEM with integrated EDS with four silicon drift detectors.

RESULTS AND DISCUSSION

Figure 1 shows mass change at 750°C/300 bar for the low impurity experiment with 50 ppm O_2 and 50 ppm H_2O additions to RG sCO_2 compared to a similar exposure in IG sCO_2. The mass change from 3-4 specimens in impure sCO_2 is shown using box and whisker plots where the whiskers show the minimum and maximum values. The lines connect the median values for each alloy. For clarity, only the dashed lines connecting the median values for 7-10 specimens in IG sCO_2 are shown. In most cases, only minor differences between the two environments were observed. The exception was the Fe-based alloy 25, which showed a higher initial mass gain in IG sCO_2. However, the subsequent rate of mass gain was very similar in the two environments. As observed previously [10,13,16,17], the mass gains were highest for the alloy 282 specimens because of the high level of Ti in this alloy (Table 1) which contains a high γ' fraction [18]. Previous work has shown that Ti accelerates the growth of the Cr_2O_3 scale [21,22]. Likewise, the mass gain for the 740 specimens was higher than that observed for alloy 625, which contains very little Ti, similar to alloy 25.

Figure 2 compares polished cross-sections of these alloys in the two environments. Consistent with the mass change data, little difference was observed in the reaction products between

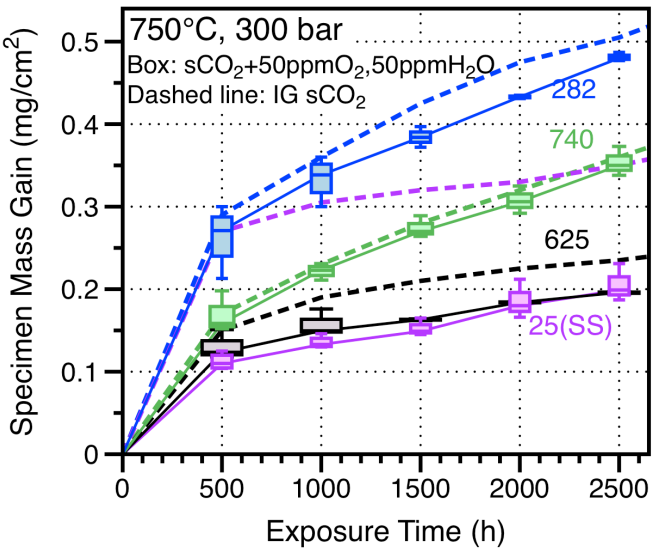

Figure 1: Specimen mass gain data for 500-h cycles at 750°C in 300 bar IG (dashed lines) and RG sCO_2 with 50ppm O_2 and 50ppm H_2O (solid lines). Box and whisker plots show data for 3-4 specimens exposed.

the two environments. Also consistent with the mass change data, the thinnest scales were observed for alloys 25 and 625 with very little internal oxidation. In contrast, the PS alloys showed thicker scales and similar internal oxidation in both environments. Previous TEM studies have shown both Ti and Al internally oxidized in 282 with Ti enriched in the scale at both the gas and metal interfaces [23].

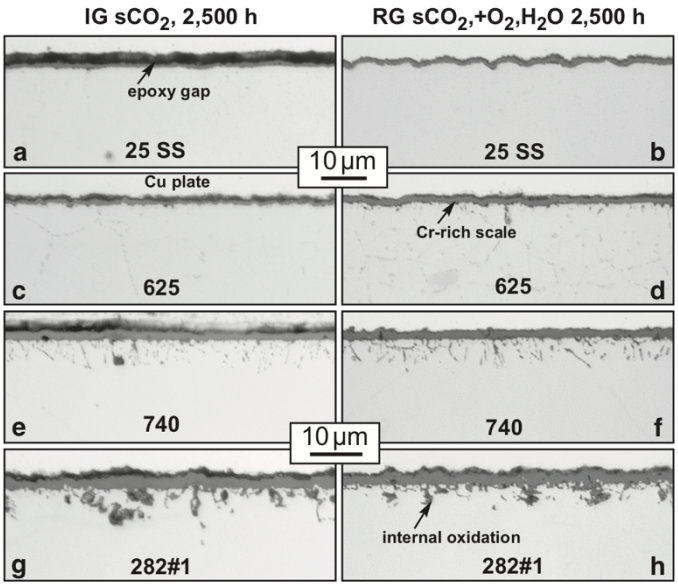

Figure 2: Light microscopy of polished cross-sections of specimens exposed for 2,500 h at 750°C/300 bar in IG sCO_2 and RG sCO_2 with 50 ppm O_2 and 50 ppm H_2O additions.

DOI:10.17185/duepublico/48899

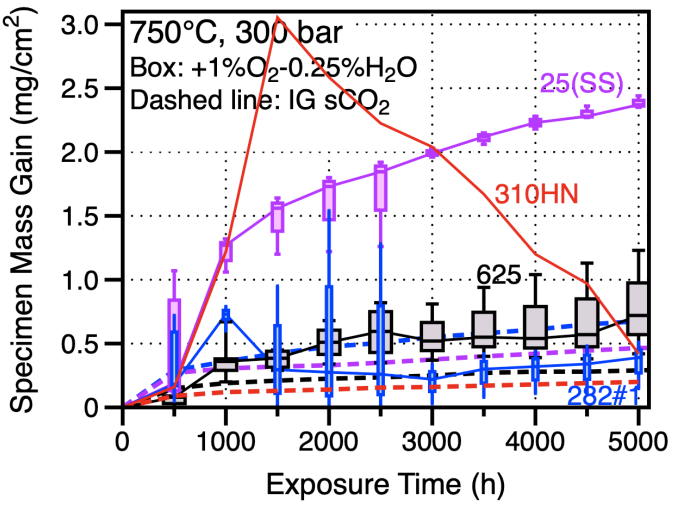

Figure 3: Specimen mass gain data for 500-h cycles at 750°C in 300 bar IG (dashed lines) and RG sCO_2 with 1% O_2 and 0.25% H_2O (solid lines). Box and whisker plots show data for 3-5 specimens exposed in the high impurity environment [17].

Similar to Figure 1, Figure 3 shows the mass change data at 750°C/300 bar for IG sCO_2 (dashed lines) and RG sCO_2 with 1%O_2 and 0.25%H_2O (solid lines and boxes) [17]. The mass gains were consistently higher for all of the materials but, particularly for the Fe-based alloys 25 and 310HN, there was a much larger increase and the drop in mass for 310HN suggested scale spallation. As all of the exposures were conducted for at least 2,500 h, Figure 4 tries to compare all of the mass change data for the four 300 bar exposures at 2,500 h [17]. As a baseline, the values are compared to a similar exposure in laboratory air. For many of the Ni-based alloys, the mass changes were very similar in all five environments. For the high impurity case, the largest mass gains were noted for the Fe-based alloys and for the alumina-forming superalloy 247.

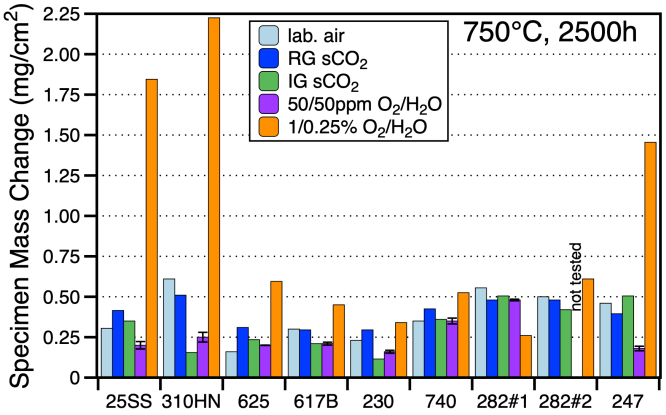

Figure 4: Median specimen mass gain values after 2,500 h exposures at 750°C in four different 300 bar environments compared to laboratory air exposures.

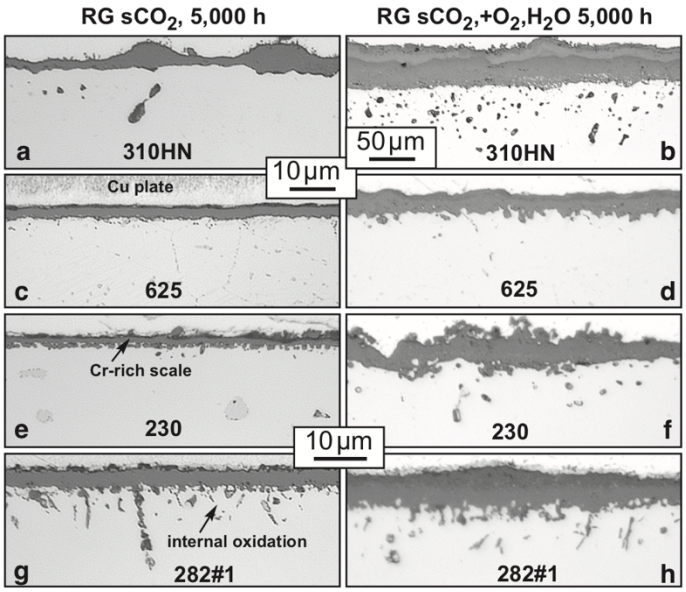

Figure 5: Light microscopy of polished cross-sections of specimens exposed for 5,000 h at 750°C/300 bar in RG sCO_2 and RG sCO_2+1%O_2+0.25%H_2O.

Figure 5 compares the reaction products in RG sCO_2 and sCO_2 with 1%O_2 and 0.25%H_2O after 5,000 h exposures. Characterization for alloys 247 and 25 after 2,500 h was studied in more detail and reported earlier [17]. Consistent with the mass change data, the oxide was thicker for all of the specimens with the addition of impurities. However, the major change for the 310HN specimen required a different magnification. SEM analysis of this specimen is in progress. For the Ni-based alloys, despite the increase, the oxide scales were still relatively thin. Figure 6 attempts to compare the scale thicknesses for each of the alloys after 5,000 h exposures in RG sCO_2 and RG sCO_2 with 1%O_2 and 0.25%H_2O. Similar to the mass change data, the results for alloys 25, 310HN and 247 are more significant.

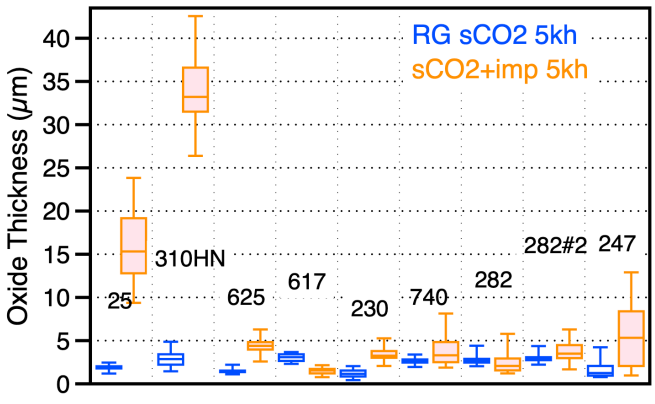

Figure 6: Box and whisker plots of the oxide scale thicknesses formed after 5,000 h at 750°C at 300 bar in RG sCO_2 (open boxes) and RG sCO_2+1%O_2+0.25%H_2O (shaded boxes).

DOI:10.17185/duepublico/48899

Because of the thin reaction products formed on most of the alloys in these environments at 750°C, conventional characterization can be challenging. Therefore, analytical TEM was used to characterize the reaction products after exposure to the environments with intentional impurity additions. To build upon prior TEM work [23,24], alloy 625 was chosen for this analysis. The scale formed on alloy 282 was found to be extremely complicated and difficult to interpret because of the incorporation of Ti and Al into the reaction product [23]. Figure 7 shows an example of the scale formed after 1,000 h at 750°C in RG sCO_2 with 50 ppm additions of O_2 and H_2O. Similar to previous observations for alloy 625 after 1,000 h in IG sCO_2, the Cr_2O_3 scale contained a mixture of large and small grains [23]. Much larger Cr_2O_3 grains formed in laboratory air after a similar exposure. Also similar to previous observations, large Mo- and Nb-rich precipitates were observed at the metal-scale interface. These precipitates are typical for the oxidation of alloy 625 where Mo and Nb are rejected from the reaction front as Cr is selectively oxidized [25]. Figure 8 shows EDS maps of the same area as shown in Figure 7. Primarily a Cr-rich oxide scale was formed. The Mo- and Nb-rich precipitates are prominent in this particular location, Figures 8c and 8d. The void at the metal-oxide interface also has been widely observed after sCO_2 exposures [26]. The low level of impurities added to this experiment appears to have had very little effect on the reaction products which is consistent with the mass change in Figure 1 and the light microscopy of the thin reaction product in Figure 2.

In contrast, Figure 9 shows a similar BF-STEM image of the scale formed on an alloy 625 specimen after 1,000 h at 750°C in RG sCO_2+1%O_2+0.25%H_2O. The magnification is not the same in Figures 7 and 9. The average oxide thickness in the FIB

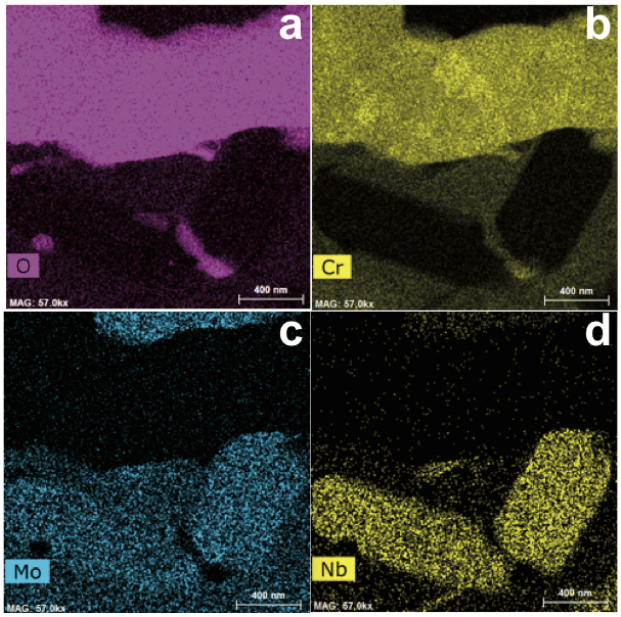

Figure 8: EDS elemental maps associated with the image in Figure 7 of the scale formed on alloy 625 after 1,000 h at 750°C in RG sCO_2 with 50 ppm additions of O_2 and H_2O, (a) O, (b) Cr, (c) Mo and (d) Nb.

TEM sections have increased from 0.8±0.06 µm with low impurity additions to 3.7±0.4 µm with high impurity levels. The EDS maps in Figure 10 indicate that the scale is enriched in Cr. However, the layer of Mo- and Nb-rich precipitates in Figure 7 appears to have been incorporated into the scale and in some

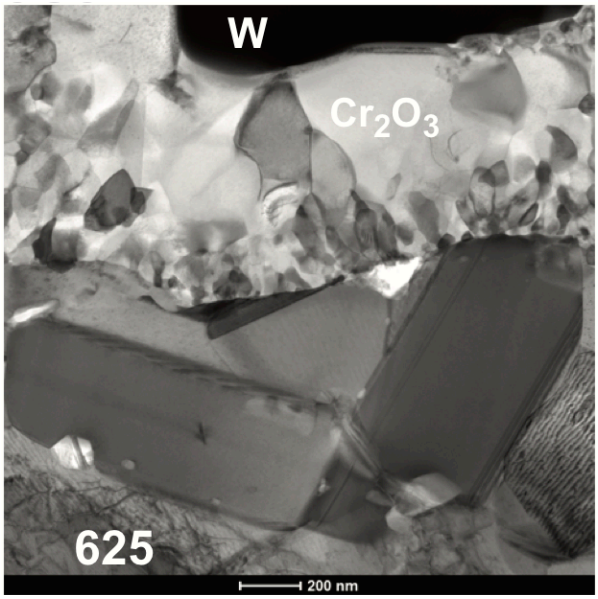

Figure 7: BF-STEM cross-sectional image of the scale formed on alloy 625 after 1,000 h at 750°C in 300 bar RG sCO_2 with 50 ppm additions of O_2 and H_2O.

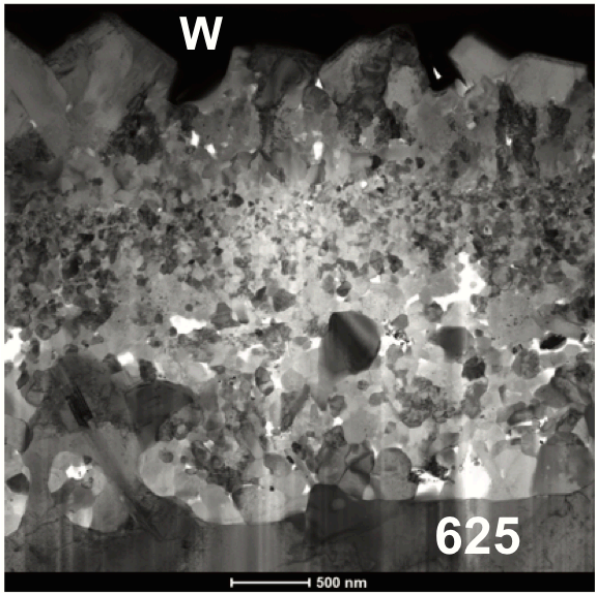

Figure 9: BF-STEM cross-sectional image of the scale formed on alloy 625 after 1,000 h at 750°C in 300 bar RG sCO_2 with additions of 1% O_2 and 0.25% H_2O.

DOI:10.17185/duepublico/48899

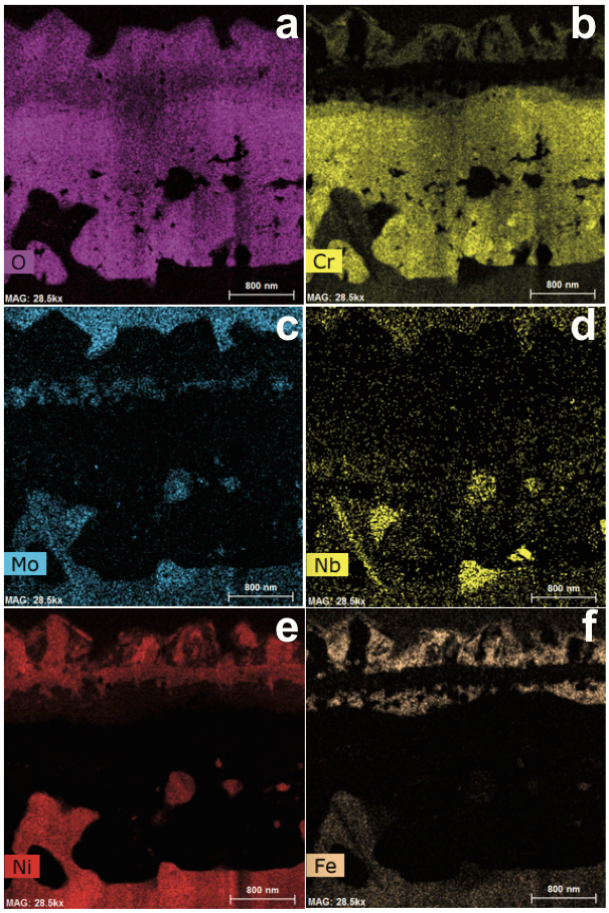

Figure 10: EDS elemental maps associated with the image in Figure 9 of the scale formed on alloy 625 after 1,000 h at 750°C in RG sCO_2+1%O_2+0.25%H_2O, (a) O, (b) Cr, (c) Mo, (d) Nb, (e) Ni and (f) Fe.

cases consumed by the reaction front. In addition, the outer part of the scale appears to be enriched in Ni and Fe. When a thicker scale is reported, it is not surprising to see oxidation of the base metal, often with the formation of an outer spinel-type MCr_2O_4 oxide layer. However, in this case the increased scale thickness is primarily due to a thicker Cr-rich layer with the Fe- and Ni-enriched layer being a relatively minor contribution. Because alloy 625 only contains only 4% Fe (Table 1), it is somewhat surprising to see Fe in the scale of a Ni-based alloy. It cannot be ruled out that the Fe may be from cross-contamination of the adjacent Fe-based alloy specimens in the autoclave experiment. Additional work is needed to rule out such a mechanism. No similar Fe enrichment was observed for the specimen shown in Figure 7 or after exposure in IG sCO_2 [23,24].

The strong effect of high levels of impurities at 750°C/300 bar on the Fe-based alloys suggests that similar studies should be conducted on Fe-based alloys at lower temperatures where they may be used to lower costs of the sCO_2 hardware. It is already clear that CO_2 restricts the use of steels to a larger degree than steam environments [27]. For example, while CSEF Grade 91 steel (Fe-9Cr-1Mo) is restricted to ~580°C in steam due to scale exfoliation issues [28], it is restricted to ~450°C due to internal carburization issues. Similar restrictions for steels might be further changed with the addition of impurities. For low impurity levels, the 50 ppm additions of O_2 and H_2O were selected to reflect the upper bound of impurities in IG CO_2. The minor effects of 50 ppm O_2 and H_2O additions suggests that these levels of impurities do not increase the oxidation rate at 750°C. This observation is consistent with the similar behavior of structural alloys in RG and IG sCO_2, Figure 4, despite the possibly higher levels of O_2 and H_2O in the latter. It could be speculated that the higher transient mass gain of the alloy 25 specimens in Figure 1 could be due to the higher impurity levels in IG sCO_2, but a similar increase was not observed when the O_2 and H_2O were intentionally added.

Considerable work remains to understand the mechanism by which these high impurity levels affect the reaction in sCO_2 and especially to isolate the roles of O_2 and H_2O. With the new experimental capability, it will now be possible to explore a wider range of impurity levels and determine the critical O_2 and H_2O levels where accelerated reaction rates are observed.

SUMMARY

For both direct- and indirect-fired supercritical CO_2 (sCO_2) cycles, impurities may be a concern. For indirect applications, comparison 500-h cyclic exposures were conducted at 750°C and 300 bar with RG and IG sCO_2 and the results were compared to RG sCO_2 with intentional additions of 50 ppm O_2 and 50 ppm H_2O. For both commercial Fe- and Ni-based structural alloys, mass changes and reaction products were unchanged with the impurity additions consistent with observed similarities between RG and IG sCO_2 experiments.

For higher impurity levels associated with direct-fired cycles, all of the alloys were somewhat affected by exposure to sCO_2+1%O_2+0.25%H_2O at 750°C/300 bar. The most significant effects were documented for the Fe-based alloys and the alumina-forming superalloy 247 after 5,000 h exposures. TEM characterization of the scales formed on 625 showed a much thicker Cr-rich oxide formed with the high impurity levels.

These results for high impurity levels are so different than prior results in ambient pressures that it is concluded that screening Fe-based alloys at a range of temperatures (400-700°C) is warranted to determine how impurities may affect sCO_2 compatibility at relevant pressures.

NOMENCLATURE

AUSC - U.S. Advanced Ultra-supercritical Steam Consortium
BF – bright field
CSEF – creep strength enhanced ferritic
CSP – concentrating solar power
EDS – energy dispersive x-ray spectrometer
GDOES – glow discharge optical emission spectrometer
FEI – electron microscope company
FIB – focused ion beam
ICP – inductively coupled plasma
IG – industrial grade

DOI:10.17185/duepublico/48899

PS – precipitation strengthened
RG – research grade
sCO_2 – supercritical carbon dioxide
SEM – scanning electron microscopy
SS – solid solution strengthened
STEM – scanning transmission electron microscopy
TEM – transmission electron microscopy

ACKNOWLEDGEMENTS

The authors would like to thank M. Howell, M. Stephens, T. M. Lowe, R. G. Brese and T. Jordan for assistance with the experimental work. Material was provided by Haynes International, Special Metals, Sandvik and Capstone Turbine, Corp. S. S. Raiman and R. Pillai provided helpful comments on the manuscript. This research was sponsored by the U.S. Department of Energy, Office of Fossil Energy, Crosscutting Technology Program and the Office of Energy Efficiency and Renewable Energy, Solar Energy Technology Program: SuNLaMP award number DE-EE0001556.

REFERENCES

[1] V. Dostal, P. Hejzlar and M. J. Driscoll, "High-Performance Supercritical Carbon Dioxide Cycle for Next-Generation Nuclear Reactors," Nuclear Technology, 154 (3) (2006) 265-282.
[2] H. Chen, D. Y. Goswami and E. K. Stefanakos, "A review of thermodynamic cycles and working fluids for the conversion of low-grade heat," Renewable & Sustainable Energy Reviews 14 (2010) 3059-3067.
[3] B. D. Iverson, T. M. Conboy, J. J. Pasch and A. M. Kruizenga, "Supercritical CO_2 Brayton cycles for solar-thermal energy," Applied Energy, 111 (2013) 957-970.
[4] R. J. Allam, M. R. Palmer, G. W. Brown Jr., J. Fetvedt, D. Freed, H. Nomoto, M. Itoh, N. Okita, C. Jones Jr., "High efficiency and low cost of electricity generation from fossil fuels while eliminating atmospheric emissions, including carbon dioxide," Energy Procedia 37 (2013) 1135–1149.
[5] P. C. Rowlands, J. C. P. Garrett, L. A. Popple, A. Whittaker, A. Hoaskey, "The oxidation performance of Magnox and advanced gas-cooled reactor steels in high pressure CO_2," Nuclear Energy 25 (1986) 267-275.
[6] Y. Gong, D. J. Young, P. Kontis, Y. L. Chiu, H. Larsson, A. Shin, J. M. Pearson, M. P. Moody and R. C. Reed, "On the breakaway oxidation of Fe9Cr1Mo steel in high pressure CO_2," Acta Materialia, 130 (2017) 361-374.
[7] E. G. Feher, "The Supercritical Thermodynamic Power Cycle," Energy Conversion, 8 (1968) 85-90.
[8] M. W. Dunlevy, "An Exploration of the Effect of Temperature on Different Alloys in Supercritical Carbon Dioxide Environment," M.Sc. Thesis, MIT, Cambridge, MA, 2009.
[9] V. Firouzdor, K. Sridharan, G. Cao, M. Anderson and T. R. Allen, "Corrosion of a stainless steel and nickel-based alloys in high temperature supercritical carbon dioxide environment," Corrosion Science 69 (2013) 281-291
[10] B. A. Pint and J. R. Keiser, "Initial Assessment of Ni-Base Alloy Performance in 0.1 MPa and Supercritical CO_2," JOM 67(11) (2015) 2615-2620.
[11] R. I. Olivares, D. J. Young, P. Marvig and W. Stein, "Alloys SS316 and Hastelloy-C276 in Supercritical CO_2 at High Temperature," Oxid. Met. 84 (2015) 585–606.
[12] J. Mahaffey, D. Adam, A. Brittan, M. Anderson and K. Sridharan, "Corrosion of Alloy Haynes 230 in High Temperature Supercritical Carbon Dioxide with Oxygen Impurity Additions," Oxidation of Metals 86 (2016) 567-580
[13] B. A. Pint, R. G. Brese and J. R. Keiser, "Effect of Pressure on Supercritical CO_2 Compatibility of Structural Alloys at 750°C," Materials and Corrosion, 68 (2017) 151-158.
[14] J. Mahaffey, A. Schroeder, D. Adam, A. Brittan, M. Anderson, A. Couet and K. Sridharan, "Effects of CO and O_2 Impurities on Supercritical CO_2 Corrosion of Alloy 625," Metallurgical and Materials Transactions A 49 (2018) 3703-3714.
[15] S. C. Kung, J. P. Shingledecker, I. G. Wright, A. S. Sabau, B. M. Tossey, and T. Lolla, "Corrosion of Heat Exchanger Alloys in Open-Fired sCO_2 Power Cycles," in Proceedings of the 6th International Symposium on Supercritical CO_2 Power Cycles, Pittsburgh, PA, March 2018, Paper #5.
[16] B. A. Pint and J. R. Keiser, "Effect of Pressure and Thermal Cycling on Long-Term Oxidation in Supercritical CO_2," NACE Paper C2019-12750, Houston, TX, presented at NACE Corrosion 2019, Nashville, TN, March 2019
[17] B. A. Pint, J. Lehmusto, M. J. Lance and J. R. Keiser, "The Effect of Pressure and Impurities on Oxidation in Supercritical CO_2," Mater. Corr. (2019) DOI:10.1002/maco.201810652
[18] L. M. Pike, "Development of a Fabricable Gamma-Prime (γ') Strengthened Superalloy," in *Superalloys 2008*, R. C. Reed et al. eds. TMS, Warrendale, PA, 2008, p.191-200
[19] J. P. Shingledecker and G. M. Pharr, "Testing and Analysis of Full-Scale Creep-Rupture Experiments on Inconel Alloy 740 Cold-Formed Tubing," J. Mater. Eng. Performance, 22 (2013) 454-462.
[20] R. Viswanathan, J. Shingledecker and R. Purgert, "Evaluating Materials Technology for Advanced Ultrasupercritical Coal-Fired Plants," Power, 154(8) (2010) 41-45.
[21] P. J. Ennis and W. J. Quadakkers, "Corrosion and Creep of Nickel-Base Alloys in Steam Reforming Gas," in High Temperature Alloys, Their Exploitable Potential, eds. J. B. Marriott, M. Merz, J. Nihoul and J. Ward, 1985, Elsevier, London, p.465-474.
[22] M. P. Brady, B. A. Pint, Z. G. Lu, J. H. Zhu, C. E. Milliken, E. D. Kreidler, L. Miller, T. R. Armstrong and L. R. Walker, "Comparison of Oxidation Behavior and Electrical Properties of Doped NiO- and Cr2O3-Forming Alloys for Solid Oxide Fuel Cell Metallic Interconnects," Oxidation of Metals, 65 (2006) 237-61.
[23] B. A. Pint, K. A. Unocic, R. G. Brese and J. R. Keiser, "Characterization of Chromia Scales Formed in Supercritical Carbon Dioxide," Materials at High Temperature 35 (2018) 39-49.

DOI:10.17185/duepublico/48899

[24] B. A. Pint and K. A. Unocic, “The Effect of CO_2 Pressure on Chromia Scale Microstructure at 750°C,” JOM 70 (2018) 1511-1519.
[25] A. Chyrkin, P. Huczkowski, V. Shemet, L. Singheiser and W. J. Quadakkers, “Sub-Scale Depletion and Enrichment Processes During High Temperature Oxidation of the Nickel Base Alloy 625 in the Temperature Range 900-1000°C,” Oxid. Met. 75 (2011) 143-166.
[26] R. P. Oleksak, J. H. Tylczak, C. S. Carney, G. R. Holcomb and O. N. Dogan, “High-Temperature Oxidation of Commercial Alloys in Supercritical CO_2 and Related Power Cycle Environments,” JOM 70 (2018) 1527-1534.
[27] S. Sarrade, D Férona, F. Rouillard, S. Perrin, R. Robin, J.-C. Ruiz, H.-A. Turc, “Overview on corrosion in supercritical fluids,” J. of Supercritical Fluids 120 (2017) 335–344.
[28] N. Nishimura, N. Komai, Y. Hirayama, and F. Masuyama, "Japanese experiences with steam oxidation on advanced heat-resistant steel tubes in power boilers," Materials at High Temperatures, 22, 3-10 (2005).

DOI:10.17185/duepublico/48899

DOI: 10.17185/duepublico/48899
URN: urn:nbn:de:hbz:464-20191004-123229-7